Adoptive Transfer of Anti-Nucleolin T Cells Combined with PD-L1 Inhibition against Triple-Negative Breast Cancer

Suyanee Thongchot[1,2], Niphat Jirapongwattana[1], Piriya Luangwattananun[2,3], Wannasiri Chiraphapphaiboon[2,4], Nisa Chuangchot[1,2], Doonyapat Sa-nguanraksa[5], Pornchai O-Charoenrat[6], Peti Thuwajit[1], Pa-thai Yenchitsomanus[2], and Chanitra Thuwajit[1]

ABSTRACT

Dendritic cell (DC)–based T-cell activation is an alternative immunotherapy in breast cancer. The anti-programmed death ligand 1 (PD-L1) can enhance T-cell function. Nucleolin (NCL) is overexpressed in triple-negative breast cancer (TNBC). The regulation of PD-L1 expression through autophagy and the anti–PD-L1 peptide to help sensitize T cells for NCL-positive TNBC cell killing has not been evaluated. Results showed the worst clinical outcome in patients with high NCL and PD-L1. Self-differentiated myeloid-derived antigen-presenting cells reactive against tumors presenting NCL or SmartDCs-NCL producing GM-CSF and IL-4, could activate NCL-specific T cells. SmartDCs-NCL plus recombinant human ribosomal protein substrate 3 (RPS3) successfully induced maturation and activation of DCs characterized by the reduction of CD14 and the induction of CD11c, CD40, CD80, CD83, CD86, and HLA-DR. Interestingly, SmartDCs-NCL plus RPS3 in combination with anti–PD-L1 peptide revealed significant killing activity of the effector NCL-specific T cells against NCL^{High}/$PD\text{-}L1^{High}$ MDA-MB-231 and NCL^{High}/$PD\text{-}L1^{High}$ HCC70 TNBC cells at the effector: a target ratio of 5:1 in 2-D and 10:1 in the 3-D culture system; and increments of IFNγ by the ELISpot assay. No killing effect was revealed in MCF-10A normal mammary cells. Mechanistically, NCL-specific T-cell–mediated TNBC cell killing was through both apoptotic and autophagic pathways. Induction of autophagy by curcumin, an autophagic stimulator, inhibited the expression of PD-L1 and enhanced cytolytic activity of NCL-specific T cells. These findings provide the potential clinical approaches targeting NCL^{High}/$PD\text{-}L1^{High}$ TNBC cells with NCL-specific T cells in combination with a PD-L1 inhibitor or autophagic stimulator.

Introduction

Triple-negative breast cancer (TNBC) is a subtype of breast cancer characterized with no estrogen, progesterone or EGFRs leading to no targeted therapies. Patients with TNBC have a poor prognosis and high relapse rates (1). Chemotherapy and radiotherapy are the approved treatments for these patients (2). Currently, TNBC shows a high expression of programmed death-ligand 1 (PD-L1) influencing patient prognosis and highlighting the potential for anti–PD-L1 immunotherapy (3).

The conventional dendritic cells (ConvDC) produced from activated monocytes by exogenous cytokines have been shown to have T-cell activation and cancer killing ability, but have several limitations in their production, that is, high cost, poor consistency, and *ex vivo* low viability (4, 5). To solve these weaknesses, researchers have developed multifunctional DC precursor cells to produce GM-CSF/IL-4 and to present tumor antigens by themselves, called self-differentiated myeloid-derived antigen-presenting cells (APC) reactive against tumors (SmartDC) that can display greater cell viability and immune potency to enhance T-cell expansion and cytotoxicity against cancers than ConvDCs (5–7). Interestingly, a toll-like receptor 4–binding protein, 40S ribosomal protein S3 (RPS3) has recently been shown to induce DCs maturation and activation, followed by increasing IFNγ-producing $CD8^+$ T-cell production and tumor destruction in the mouse model (8).

Nucleolin (NCL) is a 100–110-kDa protein that is ubiquitously expressed in exponentially growing eukaryotic cells (9). Although more than 90% of NCL is found in the nucleolus, NCL has been divided into nuclear, cytoplasmic, and cell surface NCL, depending on location in the cells (10). Reportedly, NCL has been targeted in preclinical and clinical trials of many cancers, including renal cell carcinoma (11), acute myelogenous leukemia (12), breast cancer (13), and advanced/refractory cancers with multiple metastatic sites (14). In TNBC, positive cases of NCL have been reported at around 80% (15). NCL is overexpressed and associated with the highly tumorigenic TNBC cells, metastasis, tumor relapse, poor disease prognosis, and evasion of success with standard chemotherapy (16). Inhibition of NCL using aptamers could reduce breast cancer cell aggressiveness both *in vitro* and *in vivo* (15). In a current review of literature, no NCL-specific T cells have revealed their effects on TNBC cell killing.

[1]Department of Immunology, Faculty of Medicine Siriraj Hospital, Mahidol University, Bangkok, Thailand. [2]Research Department, Siriraj Center of Research Excellence for Cancer Immunotherapy (SiCORE-CIT), Faculty of Medicine Siriraj Hospital, Mahidol University, Bangkok, Thailand. [3]Division of Molecular Medicine, Research Department, Faculty of Medicine Siriraj Hospital, Mahidol University, Bangkok, Thailand. [4]Department of Biochemistry, International Graduate Program in Medical Biochemistry and Molecular Biology, Faculty of Medicine Siriraj Hospital, Mahidol University, Bangkok, Thailand. [5]Department of Clinical Surgery, Faculty of Medicine Siriraj Hospital, Mahidol University, Bangkok, Thailand. [6]Breast Center, Medpark Hospital, Bangkok, Thailand.

Note: Supplementary data for this article are available at Molecular Cancer Therapeutics Online (http://mct.aacrjournals.org/).

Corresponding Author: Chanitra Thuwajit, Faculty of Medicine Siriraj Hospital, Mahidol University 10700 Thailand. Phone: 66-2-418-0569; Fax: 66-2-418-1636; E-mail: chanitra.thu@mahidol.ac.th

Mol Cancer Ther 2022;21:727–39

doi: 10.1158/1535-7163.MCT-21-0823

The alterations in autophagy are involved in tumor survival-promoting or tumor-suppressing mechanisms (17). Autophagy impairment such as low expression of BECLIN-1 was strongly associated with poor prognosis and an independent predictor of survival of basal-like and HER2-enriched breast cancers (18). The deficiency in the autophagy pathway has been associated with defects in T cell-mediated killing in TNBC tumors (19). Activation of autophagy significantly suppressed PD-L1 (20). The combination of anti–PD-L1 antibody with an autophagic stimulator bisdemethoxycurcumin showed the reduction of bladder cancer cell viability by the action of T cells (21–23).

In this present study, NCL-specific T cells were produced using SmartDCs and killing capability of these T cells on NCL^{High}/$PD\text{-}L1^{High}$ TNBC cells was increased by direct targeting PD-L1 using anti–PD-L1 peptide or indirect controlling PD-L1 expression by curcumin, an autophagic stimulator. High NCL and PD-L1 in patients with TNBC revealed a significant correlation with short patient survival time. The production of monocyte-derived SmartDCs-NCL was performed by transduction of healthy donor peripheral blood mononuclear cells (PBMC)-derived monocytes with a GM-CSF/IL-4/NCL tricistronic lentiviral system. RPS3 was added and showed a significantly higher SmartDCs maturation leading to NCL-specific T cell activation and killing of NCL^{High} TNBC cells. The anti–PD-L1 peptide could sensitize NCL-specific T cells against NCL^{High}/$PD\text{-}L1^{High}$ TNBC cells. Interestingly, curcumin could suppress PD-L1 production on cancer cells through p62-mediated autophagy leading to the sensitization of NCL-specific T cells to destroy NCL^{High}/$PD\text{-}L1^{High}$ TNBC cells.

Materials and Methods

Antibodies and Reagents

The primary antibodies used for IHC, immunofluorescence (IF), Western blotting (WB), and flow cytometry (FC) are listed: Rabbit polyclonal anti-NCL antibody (IHC 1:50; IF 1:50, WB 1:500, FC 1:50, #14574, Cell Signaling Technology, Inc.) or rabbit anti–PD-L1 antibody (IHC 1:50; IF 1:50, WB 1:1,000, FC 1:50, ab205921, Abcam) or rabbit anti-LC3 (IF 1:100; WB 1:2,000, L7543, Sigma-Aldrich Corporation) or mouse anti-SQSTM1/p62 (IF 1:50; WB 1:500, sc-28359, Santa Cruz Biotechnology, Inc.) or mouse anti-BAX (IF 1:100: WB 1:1,000, #610983, Becton Dickinson Holdings PTE. Ltd.) or rabbit anti–BCL-2 (WB 1:2,000, ab196495, Abcam) or β-actin (WB 1:10,000, sc-47778, Santa Cruz Biotechnology). Horseradish peroxidase (HRP)–conjugated goat anti-mouse (1:2,000) and goat anti-rabbit (1:2,000), both from Bio-Rad, were used as secondary antibodies for WB. Goat anti-rabbit IgG-FITC antibody (1:2,000, ab6717, Abcam) and goat anti-mouse IgG-Cy3-AffiniPure F(ab')2 Fragment (1:2,000, #115–116–071, Jackson Immuno Research Laboratories, Inc.) were used for IF. Hoechst33342, trihydrochloride trihydrate (IF 1:1,000, Invitrogen Corporation), from Thermo Fisher Scientific Inc. was added to stain the nucleus.

The antibodies for phenotypic analysis of monocytes and DCs were bought from ImmunoTools GmbH (Friesoythe, Germany): anti-CD11c APC (1:50, #21487116), anti-CD14 FITC (1:50, #21620143), anti-CD40 FITC (1:50, #21270403), and anti-HLA-DR FITC (1:50, #21278993); anti-CD80 PE (1:50, #12–0809–42), anti-CD83 PE (1:20, #12-0839-42) and anti-CD86 PE (1:20, #12-0869-42; Thermo Fisher Scientific, Inc.). The antibodies for T-cell subsets were purchased from Thermo Fisher Scientific Inc.: FITC-conjugated anti-CD3 (1:50, #48–0037–41), anti-CD4 Alexa Fluor 700 (1:50, #56–0049–42) and anti-CD8 APC-Cy7 (1:50, #A15448); anti-CD45RA APC (1:50, #21279456) and anti-CD62 L PE (1:50, #21819624) from ImmunoTools GmbH.

HLA typing of healthy donors was performed using anti-HLA-A2 APC (1:50, #17-9876-42, ImmunoTools GmbH). Anti–PD-L1 peptide (CLQKTPKQC; ref. 24) and NCL peptides (KMAPPPKEV and VLSNLSYSA) restricted to HLA-A*02 were synthesized from GenScript Biotech PTE. LTD. (Galaxis West Lobby). Curcumin (Merck-Schuchardt) was kindly provided by Prof. Somchai Pinlaor, Khon Kaen University. Spautin-1 (1262888–28–7, Sigma-Aldrich) was kindly provided by Prof. Ciro Isidoro, Università del Piemonte Orientale "A. Avogadro," Italy.

Cell lines and cell culture

The human embryonic kidney cells (HEK) 293T (Lenti-X 293T-cell, #632180; Takara Bio USA, Inc.) and human breast cancer cell lines, MDA-MB-231 (#HTB-26) and MCF-7 (#HTB-22) were purchased from the ATCC and cultured in DMEM (Gibco, Thermo Fisher Scientific Inc.) supplemented with 10% FBS (v/v; Gibco), 100 U/mL of penicillin and 100 μg/mL of streptomycin (Sigma-Aldrich). HCC70 (#CRL-2315, ATCC) was cultured in RPMI-1640 (Gibco). MCF-10A (#CRL-10317, ATCC) was cultured in DMEM supplemented with 5% horse serum (Invitrogen Corporation), 100 U/mL of penicillin and 100 μg/mL of streptomycin, 20 ng/mL EGF (PeproTech), 0.5 mg/mL hydrocortisone (Sigma-Aldrich), 100 ng/mL cholera toxin (Sigma-Aldrich), and 10 μg/mL insulin (Sigma-Aldrich). All cells were maintained at 37°C in 5% CO_2 incubator. The cell viability was measured at each passage using a standard trypsinization protocol. Cells were passaged every 3 to 4 days to maintain a confluence rate of 20%–80% and then passaged a maximum of 10 times when experiments were performed. All cell lines used in the study have been routinely tested every 6 months for negative mycoplasma as determined by the *Mycoplasma* nested PCR primer set (BioDesign Co., Ltd.) throughout the study. The HLA typing of two breast cancer cell lines were followed: MDA-MB-231 (A*02:01, 02:17; B*40:02,41:01; C*02:02,02:17; ref. 25); https://web.expasy.org/cellosaurus/CVCL_0062 and HCC70 (A*30:02,03:01; B*78:01,15:16; C*16:01,16:01; ref. 26); https://web.expasy.org/cellosaurus/CVCL_1270).

IHC staining of NCL and PD-L1 in breast cancer tissues

NCL and PD-L1 proteins were detected on the paraffin-embedded tumor microarray of 144 cases under the approval of sample collection and usage from Siriraj Institutional Review Board (COA no. Si 580/2018). In brief, 4-μm-thick sections were incubated with primary antibodies overnight in a humidified chamber at 4ºC and then with rabbit Envision^{+}System HRP-labeled polymer IHC secondary antibody (K4003, DAKO) for 30 minutes at RT (room temperature). The peroxidase activity was visualized with diaminobenzidine (DAB) solution and counterstained by hematoxylin. The staining proteins were quantitatively scored by scanning the slides with 3DHistech Ltd. CaseViewer/QuantCenter software 2.4.0. (Sysmex) and scored on the basis of the percentages of positive cells: 0%, negative; 1%–25%, +1; 26%–50%, +2; 51%–75%, +3; and 76%–100%, +4. The intensity of protein staining was scored as weak, 1; moderate, 2; and strong, 3. The IHC scores were calculated by multiplying the positive cell score with the intensity score resulting to 0–12 IHC scores, which were used to classify the samples into two groups: low expression levels; scores <6 and high expression levels; sores ≥6.

IF staining of cell lines

MDA-MB-231, HCC70, MCF-7 and MCF-10A cell lines were cultured on sterile glass coverslips for 24 hours. Chloroquine (ClQ, C6628–25G, Sigma-Aldrich), an inhibitor of autophagosome degradation (27), was used at 30 μmol/L and added 8 hours before sample

collection. The cells were fixed in ice-cold absolute methanol. Non-specific protein binding was blocked with 3% BSA/1X PBS, then incubated overnight at 4°C in a humidified chamber with the indicated primary listed in the above paragraph. After washing, the appropriate secondary fluorescence antibody was applied for 3 hours at RT. The nuclei were stained with Hoechst33342. Fluorescence was captured with a ZEISS LSM 800 confocal laser fluorescence scanning microscope (AxioObserver7, LSM 800, Zeiss).

Western blot assay

Cells were lysed with radioimmuno-precipitation assay buffer. A protein assay was performed using the Bradford kit (Bio-Rad Laboratories). A total of 20 μg of homogenate was fractionated by SDS-PAGE and transferred to a polyvinylidene fluoride membrane (Whatman). The membranes were incubated overnight at 4°C with the primary antibody, followed by incubation with the appropriate secondary antibody at RT for 1 hour. β-Actin was used as an internal control. The immunoreactive signals were visualized by Enhanced Chemiluminescence Plus solution (Thermo Fisher Scientific) under Gel Document (Syngene). The bands were quantified by ImageJ version 1.48v (NIH, Bethesda, MD).

Construction of tricistronic vectors and lentivirus production

Lentivirus-harboring tri-cistronic (RRE-cPPT-EF-1α-mGM-CSF-P2A-mIL4-F2A-mNCL) complementary DNA sequences encoding human GM-CSF, human IL-4, and NCL protein (pCDH-GM-CSF/IL4/NCL; **Fig. 2A**) were produced as previously described (5, 6, 7). Unrelated protein, phytochrome-based near-infrared fluorescent protein (iRFP) was used as a control. Large-scale production was performed by transient co-transfection of Lenti-X 293T cells as previously described (5). Lentiviral titers were determined by quantifying the Lenti-X p24 Rapid Titer kit by RT-PCR (Clontech Laboratories, Inc.).

Generation of ConvDCs and SmartDCs-NCL from healthy donors

PBMCs from HLA-A*02–positive, were isolated with Lymphocyte separating medium (Corning). This present study was approved by Siriraj Institutional Review Board (COA no. Si 580/2018) and conducted in accordance with the Declaration of Helsinki. The written informed consent was obtained from all healthy donors. On day 0, PBMCs (1×10^6/well) were plated in 12-well plates (Corning). For ConvDCs growth, the adherent monocytes were cultured in AIM-V media (Invitrogen Corporation) with GM-CSF (50 ng/m, ImmunoTools GmbH) and IL-4 (25 ng/mL, ImmunoTools GmbH; ref. 28). Transduction was carried out on day 5 of culture with LV (100 multiplicity of infection) and protamine sulfate (10 μg/mL) added to adherent monocytes and incubated for 16 hours at 37°C, the cells were replaced with AIM-V media to activate T cells. The immature DCs were cultured in AIM-V media with IFNα (50 ng/mL, ImmunoTools GmbH), IFNγ (50 ng/mL, ImmunoTools GmbH), and recombinant human RPS3 (1 μg/mL, Novus Biological) for 2 days to induce mature DCs. At day 7 of culture, the phenotypic analysis of DCs and SmartDCs was compared with monocytes performed by the CytoFLEX Flow cytometer (Beckman Coulter) and analyzed by FlowJo VX software (Tree star, Inc.).

GM-CSF, IL4, and IFNγ measurement by ELISA

For GM-CSF and IL4, culture supernatant was harvested on day 7 whereas on day 15 for IFNγ. The cytokine levels were measured by ELISA kits (R&D Systems, Inc.) followed the instruction.

Activation of effector T cells

SmartDCs-NCL or SmartDCs-iRFP or ConvDCs were used as stimulators for cryopreserved lymphocytes and resuspended in AIM-V medium supplemented with 5% human AB serum (Merck KGaA) at a ratio of lymphocytes to DCs as 10:1 for 3 days. Subsequently, the activated T cells were expanded in AIM-V medium supplemented with 5% human AB serum, IL-2 (20 ng/mL, ImmunoTools GmbH), IL-7 (10 ng/mL, ImmunoTools GmbH), and IL-15 (20 ng/mL, ImmunoTools GmbH) for 5 days. The culture media were replaced every other day.

T-cell subset analysis using flow cytometry

Activated T cells were harvested on day 15. Immunostaining was performed with commercially available fluorescent antibodies against CD3, CD4, CD8, CD42RA, CD62 L, and respective isotype controls. FC was performed by CytoFLEX (Beckman Coulter).

Enzyme-linked immunospot technique assay

Specific secretions of IFNγ from T cells in response to stimulator cells were assayed by Human IFNγ ELISpot^{BASIC} (Enzyme-linked immunospot technique) kit (Mabtech, Inc.) following the manufacturer's instructions. HLA-A*02 T2 cells (purchased from the ATCC) were pulsed with 10 μmol/L of NCL peptides (KMAPPPKEV$_{15-23}$ and VLSNLSYSN$_{488-496}$, GenScript). Cells were scanned with ELISpot plate reader (BIOREADER 5,000 Fγ, BIOSyS) and counted with CellCounter software (Nghia) version 0.2.1. Phorbol myristate acetate (PMA, P1585, Sigma-Aldrich) and ionomycin (I9657, Sigma-Aldrich) were used as positive controls.

2-D tumor cell killing

The mWasabi and CMRA fluorescence target cells (1×10^4) were seeded into 96-well plates (Corning). Effector cells were incubated with target cells at ratios of 1:1, 5:1, and 10:1. After 24 hours, target cells were measured by the Pierce Firefly Luciferase Glow Assay Kit (Thermo Fisher Scientific Inc.) and Lumat LB 9507 Ultra-sensitive Luminometer (Berthold Technologies GmbH & Co. KG.). Cancer cell lysis was calculated as:

$$\%\text{Cancer cell lysis} = 100 - \left(\frac{lucCancer^{cocultured\ activated\ T\ cells}}{lucCancer^{cocultured\ unactivated\ T\ cells}} \times 100\right)$$

3-D tumor spheroid killing

The mWasabi and CMRA fluorescence target cells or CellTracker Green CMFDA Dye–labeled target cells were formed in Ultra Low Attachment (ULA) 96-well Round-Bottom plates (Corning) at 1×10^4 cells/well in 2.5% of Matrigel (Corning). The plates were centrifuged for 3 minutes at 300 × *g* at 4°C to initiate the formation of spheroids. CellTracker Orange CMRA Dye (C2927, Thermo Fisher Scientific Inc.) or CellTracker Blue CMF2HC Dye (C12881, Thermo Fisher Scientific Inc.) labeled activated effector T cells (E) were added to target cancer cells (T) at (E:T) ratios of 1:1, 5:1, and 10:1. Fluorescence signals were detected by fluorescence inverted microscopy and CellSense Standard program version 1.15 (Olympus). The ImageJ (NIH) software was used to quantify the change in mean fluorescence intensity (MFI) relative to the spheroid inactivated T cells. Videomovie clips of cells killing up to an E:T ratio of 10:1 were performed through 30-frame images using a confocal microscope (Zeiss LSM 800, Carl Zeiss; ×63). The acquisition software was ZEN 2.3 software (Blue edition, 2002–2011).

Colony formation assay

MDA-MB-231 and MCF-7 (10,000 cells/well) were seeded in 96-well plates (Corning) and cultured overnight. T cells were added to the wells on the next day at the indicated E:T ratios for 24 hours. T cells were then removed and washed with 1X PBS, fixed with absolute methanol, stained with a 0.5% crystal violet solution. The colony number was counted by photometric measurements using CellCounter software (Nghia).

Statistical analysis

The relation between NCL and PD-L1 and clinicopathological factors were analyzed using the χ^2 test and Fisher's exact test. Survival curves were analyzed with the Kaplan–Meier method and compared using the log-rank test. Multivariate analysis of prognostic factors was evaluated in a Cox proportional hazards model. Data were presented as mean ± SD. Student *t* test and one-sided ANOVA followed by Tukey's *post hoc* test were performed for comparison of 2 samples and more than 2 samples. Statistical analyses were performed using SPSS 20.0 statistics software (SPSS, IBM) and GraphPad Prism version 7.04 software (GraphPad Software). A *P* value of less than 0.05 was considered statistically significant.

Data availability

The data generated in this study are available within the article and its Supplementary Data Files. The DNA sequence data have been deposited in GenBank and are available under accession number BankIt2554073 SmartDC-NCL OM792960.

Results

Clinicopathological and prognostic implications NCL and PD-L1 in human TNBC tissues

The expressions of NCL and PD-L1 were observed in 144 tumor microarray TNBC cases. The immunohistochemical stain for NCL showed staining pattern in both nucleolar and cytoplasmic parts whereas PD-L1 showed predominantly located in the cytoplasm with some cell membrane localization. Most of the cases had high NCL in the nucleus (109/144, 75%), whereas PD-L1 was detected at both cytoplasmic and outer membrane regions (83/144, 58%; **Fig. 1A**; Supplementary Fig. S1D). Four groups of samples were shown according to low or high of either NCL or PD-L1, including NCL^{Low}/PD-$L1^{Low}$, NCL^{Low}/PD-$L1^{High}$, NCL^{High}/PD-$L1^{Low}$ and NCL^{High}/PD-$L1^{High}$. The percentage of NCL^{Low}/PD-$L1^{Low}$ TNBC tissues was 8.3% (12/144), 13.9% (20/144) for NCL^{Low}/PD-$L1^{High}$, 14.6% (21/144) for NCL^{High}/PD-$L1^{Low}$, and the highest was 63.2% (91/144) for NCL^{High}/PD-$L1^{High}$ (Supplementary Fig. S1A; **Table 1**). Consistent with the evidence in TNBC tissues, the TNBC cell lines, MDA-MB-231 and HCC70 revealed higher levels of both NCL and PD-L1 than MCF-7 luminal breast cancer cells and MCF-10A normal mammary epithelial cells with statistical significance (**Fig. 1B**; Supplementary Fig. S1B and S1C). FC analysis confirmed high membrane PD-L1 in both MDA-MB-231 and HCC70 cells (Supplementary Fig. S1C).

Survival analysis demonstrated that high NCL or high PD-L1 were significantly associated with a short overall survival (OS) time (**Fig. 1C**; $P = 0.003$ and **Fig. 1D**; $P = 0.024$). Most importantly, the combination pattern of NCL^{Low}/PD-$L1^{Low}$ (**Fig. 1E**, blue line) was associated with a good OS whereas NCL^{High}/PD-$L1^{High}$ (**Fig. 1E**, violet line) was related to poor prognostic clinical outcomes ($P < 0.001$). The hazard ratio (HR) for death based on level of NCL or PD-L1 was 0.270 [95% confidence interval (CI), 0.148–0.494; $P < 0.001$] for NCL^{Low}/PD-$L1^{Low}$ and HR, 1.227; 95% CI, 1.299–3.341; $P = 0.002$ for NCL^{High}/PD-$L1^{High}$ (**Table 1**).

The Fisher's exact test indicated significant inverse correlations of PD-L1 and pN stage ($P = 0.034$), and clinical staging ($P = 0.010$; **Fig. 1F**); however, no statistical significance of these variable parameters with the NCL level were found. No significant differences between NCL and PD-L1 staining patterns and clinicopathological features, including age, pT stage, pM stage, LN metastasis, perineural metastasis, and size were observed (Supplementary Tables S1 and S2). The univariate analyses revealed high NCL levels as an independent poor prognostic marker (**Fig. 1G**; HR, 2.091; 95% CI, 1.405–3.113; $P = 0.000$), as well as high PD-L1 (**Fig. 1G**; HR, 1.818; 95% CI, 1.290–2.564; $P = 0.001$).

Generation and potency testing of monocyte-derived RPS3-mediated SmartDCs-NCL

Tri-cistronic LV containing GM-CSF, IL-4 and NCL (RRE-cPPT-EF-1α-**mGM-CSF**-P2A-**mIL4**-F2A-**mNCL**; **Fig. 2A**) was constructed and transfected into Lenti-X 293T cells. The LV system could successfully produce higher NCL expressions than those in the untransfected (Supplementary Fig. S2A). The immunophenotypic characteristics, of monocytes (day 0) or ConvDCs and cells transduced with LV-GMCSF-IL4-iRFP or LV-GMCSF-IL4-NCL (SmartDCs-NCL) or SmartDCs-NCL+RPS3 (day 7) were shown to have dendritic-like morphology (Supplementary Fig. S2B). All activated DCs had downregulation of CD14 and upregulation of DC markers, including CD11c, CD40, CD80, CD83, CD86, and HLA-DR compared with monocytes (Supplementary Fig. S2D). The significantly higher levels of CD40 and CD80 in SmartDCs-NCL treated with RPS3 in comparison with those of SmartDCs-NCL without RPS3 were detected (**Fig. 2B**). SmartDCs-NCL and RPS3-treated SmartDCs-NCL exhibited the expected significant increment levels of GM-CSF (**Fig. 2C**) and IL4 (**Fig. 2D**) compared with monocytes.

The characterization of effector T cells produced by SmartDCs-NCL or SmartDCs-NCL plus RPS3

The established T-cell subsets after co-culture with ConvDCs, SmartDCs-iRFP, SmartDCs-NCL or SmartDCs-NCL plus RPS3 were analyzed (**Fig. 2E**; Supplementary Fig. S2C). There were no significant differences in the percentages of $CD3^+/CD4^+$ and $CD3^+/CD8^+$ T cells expanded after being co-cultured with SmartDCs-NCL and SmartDCs-NCL plus RPS3 that markedly increased $CD3^+/CD8^+/CD45RA^-/CD62L^-$ effector memory T cells (T_{EM}; ref. 29) but were decreased in $CD3^+/CD8^+/CD45RA^-/CD62L^+$ and $CD3^+/CD8^+/CD45RA^+/CD62L^+$ characterized by late $CD45RA^+$ effector memory T cells (T_{EMRA}) and native T cells (T_N; ref. 29).

Subsequently, IFNγ was detected by ELISA assay in the culture supernatant when T cells were incubated with different DCs at a ratio 1:10. The T cells activated by SmartDCs-NCL and SmartDCs-NCL plus RPS3 showed significantly higher IFNγ reactivity against MDA-MB-231 (717.24 ± 84.48 pg/mL and 1,037.93±46.55 pg/mL) than that of unactivated T cells, ConvDCs-activated T cells, and SmartDCs-iRFP–activated T cells (**Fig. 2F**). The similar pattern of results was detected against HCC70 TNBC cells (798.28±31.03 pg/mL and 992.41 ± 89.65 pg/mL; **Fig. 2F**). No IFNγ secreted from T cells co-cultured with MCF-10A normal breast cells was observed.

To determine whether the expanded T cells were NCL-specific T cells, the HLA-A*02–restricted T2 cells were used as APCs loaded with pooled NCL peptides and then co-cultured with T cells. After 24 hours stimulations, high IFNγ spots were significantly detected in T cells

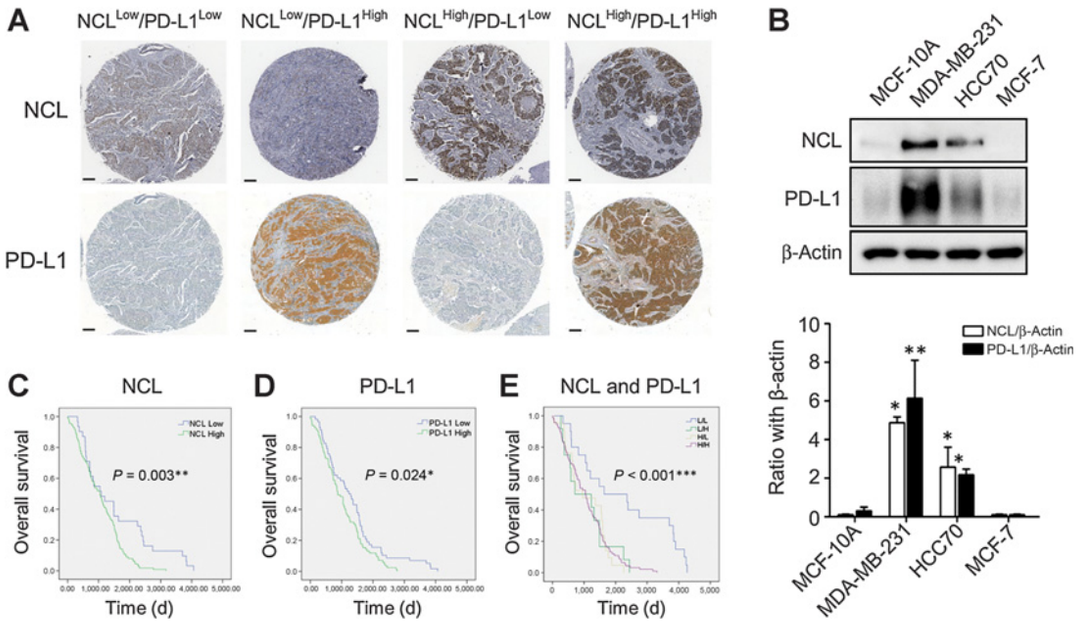

F Correlation between the expression of NCL and PD-L1 and clinico-pathological data of TNBC patient ($n = 144$)

Variable (no. of patients)	*n*	NCL IHC score		*P*	PD-L1 IHC score		*P*
		Low	High		Low	High	
pN stage							
1–2	135	34	101		80	55	
3	9	1	8	0.309	2	7	0.034*
Clinical staging							
1–2	118	28	90		73	45	
3–4	26	7	19	0.453	9	17	0.010*

G Univariate analysis by Cox proportional hazard regression model for the evaluation of prognostic factors

Variable (no. of patients)	No. of patients who died (5-year survival cutoff)	Hazard ratio (HR)	95% confidence interval (CI)	*P*
NCL IHC score				
Low	35	1		
High	109	2.091	1.405–3.113	0.000***
PD-L1 IHC score				
Low	82	1		
High	62	1.818	1.290–2.564	0.001**

Figure 1.

NCL and PD-L1 expressions and clinicopathological correlations in 144 TNBC. **A,** IHC staining of NCL and PD-L1 in breast cancer tissues (scale bar, 200 μm; original magnifications of ×50). **B,** The western blot analysis of NCL and PD-L1 expression levels in three breast cancer cells and MCF-10A normal mammary cell. β-Actin was used as an internal control. **C** and **D,** The Kaplan–Meier curves for overall survival. **E,** The pattern of NCL and PD-L1 expression (NCL^{Low}/PD-L1^{Low}, NCL^{Low}/PD-L1^{High}, NCL^{High}/PD-L1^{Low} and NCL^{High}/PD-L1^{High}) and the overall survival rates. **F,** The correlation of NCL and PD-L1 levels and patients' clinicopathological data. **G,** Univariate analysis by Cox proportional hazard regression analysis. Data are shown as mean±SD. *, $P < 0.05$; **, $P < 0.01$; and ***, $P < 0.001$.

activated by SmartDCs-NCL and SmartDCs-NCL plus RPS3, resulting in about 2.07-fold ($P = 0.015$) and 1.77-fold ($P = 0.045$) differences compared with those with no antigen peptide exposure (**Fig. 2G** and **H**). The highest number of IFNγ spots was observed in PMA/Ionomycin, a positive control condition.

Anti–PD-L1 peptide enhances NCL^{High}/PD-L1^{High} TNBC cell killing of NCL-specific T cells

The combination of NCL-specific T cells and anti–PD-L1 peptide on killing of NCL^{High}/PD-L1^{High} MDA-MB-231 and HCC70 TNBC cells was investigated. After incubation for 24 hours with target cancer

Table 1. Multivariate analysis by the Cox proportional hazard regression model for the evaluation of NCL and PD-L1 in TNBC clinical samples.

Variable (no. of patients)	Hazard ratio (HR) 95% Confidence interval (CI)	*P*
$NCL^{Low}/PD\text{-}L1^{Low}$ (13.9%, 20/144 cases)	0.270 (0.148–0.494)	<0.001***
$NCL^{Low}/PD\text{-}L1^{High}$ (8.3%, 12/144 cases)	1.249 (0.689–2.262)	0.464
$NCL^{High}/PD\text{-}L1^{Low}$ (14.6%, 21/144 cases)	1.227 (0.766–1.964)	0.394
$NCL^{High}/PD\text{-}L1^{High}$ (63.2%, 91/144 cases)	1.227 (1.299–3.341)	0.002**

Note: Multivariate analysis by Cox proportional hazard regression; 95% CI indicates 95% confidence interval; **, $P < 0.01$ and ***, $P < 0.001$ were considered statistically significant.

cells, cell death was measured and calculated as an increased percentage of specific cell lysis of mWasabi and CMRA fluorescence-labeled viable cells (**Fig. 3A–C**). NCL-specific T cells activated with SmartDCs-NCL (red bar) or SmartDCs-NCL plus RPS3 (blue bar) were significantly increased in the percentage of specific cell lysis at ratios 1:1, 5:1, and 10:1 for MDA-MB-231 cell (**Fig. 3A**) whereas an only ratio 10:1 of HCC70 was revealed (**Fig. 3B**). Adding anti–PD-L1 peptide into the co-culture of cancer cells with NCL-specific T cells, the percentages of specific cell lysis of MDA-MB-231 by NCL-specific T cells activated with SmartDCs-NCL plus RPS3 (pink bar) were significantly greater than NCL-specific T cells without anti–PD-L1 peptide (red bar; **Fig. 3A**). A similar result was detected in the condition of using only NCL-specific T cells with anti–PD-L1 peptide (green bar) compared with SmartDCs-iRFP (black bar) for both MDA-MB-231 and HCC70 cells at ratio of E:T at 10:1. No killing activities of NCL-specific T cells were detected in MCF-10A having no NCL and PD-L1 expressions (**Fig. 3C**).

3-D cancer spheroids to evaluate the potency of NCL-specific T cells were developed (**Fig. 3D–G**). The overall sphere growth rate in 2.5% Matrigel over 96 hours is shown in MDA-MB-231, HCC70, and MCF-10A cells (**Fig. 3D**). The greater antitumor efficacy of T cells against MDA-MB-231 was associated with a decreased MFI at E:T equaled 5:1 of SmartDCs-NCL+anti–PD-L1 peptide (green line, $P = 0.049$) and SmartDCs-NCL+RPS3+anti–PD-L1 peptide (pink line, $P = 0.023$) compared with that of unactivated T cells (**Fig. 3E**). At a 10:1 ratio, MDA-MB-231 cells were killed by T cells activated by SmartDCs-iRFP (black bar) less than those of SmartDCs-NCL+anti–PD-L1 peptide (green line; $P = 0.026$), as well as T cells activated by SmartDCs-NCL+RPS3+anti–PD-L1 peptide (pink line; $P = 0.003$; **Fig. 3E**). Using NCL-specific T cells in combination with only anti–PD-L1 peptide showed better killing capability than T cells alone, but without statistical significance. Interestingly, T cells in combination with RPS3 and anti–PD-L1 peptide had higher killing capability against NCL-positive cancer cells than that of T cells alone (red line; $P = 0.016$) and of T cells+anti–PD-L1 peptide ($P = 0.233$; **Fig. 3E**). In addition, 3-D HCC70 spheroids showed a significant decrease in MFI at a ratio 10:1 of SmartDCs-iRFP (black bar) versus SmartDCs-NCL+anti–PD-L1 peptide (green line, $P = 0.041$; **Fig. 3F**). No treatment-associated toxicity was detected in MCF-10A normal breast cells (**Fig. 3G**). Furthermore, the tumor killing activities of T cells activated by SmartDCs-NCL and SmartDCs-NCL+RPS3 compared with SmartDCs-iRFP and tumor alone were recorded (Supplementary Movies S1–S5). T cells activated by SmartDCs-NCL and SmartDCs-NCL+RPS3 were specifically killed and infiltrated into NCL^{High} MDA-MB-231 cells.

Curcumin-mediated autophagic degradation of PD-L1 sensitizes $NCL^{High}/PD\text{-}L1^{High}$ TNBC cell killing by NCL-specific T cells

To know how NCL-specific T cells would affect the death of $NCL^{High}/PD\text{-}L1^{High}$ TNBC cells in the actions of anti–PD-L1 peptide and an autophagy modulator, the expressions of autophagy markers, LC3 and p62 in breast cancer cells treated with NCL-specific T cells were detected. The intrinsic autophagy levels were higher in the order of MDA-MB-231 > HCC70 > MCF-7 > MCF-10A (**Fig. 4A** and **B**). The cellular levels of LC3, p62, and PD-L1 were concomitantly accumulated in chloroquine (ClQ) treatment reflecting the degradation of PD-L1 in high autophagic MDA-MB-231 cells more than those in low autophagic MCF-7 cells (**Fig. 4C**; Supplementary Fig. S3A–S3C).

The mechanism underlying anti–PD-L1 or autophagy modulator-mediated NCL-specific T cells that induced TNBC death was explored. The induction of autophagy (increasing the LC3-II/I ratio) and apoptosis (increasing the BAX/BCL-2 ratio) was observed in MDA-MB-231 treated with NCL-specific T cells activated by SmartDCs-NCL+curcumin (**Fig. 4D**, lane 5) > SmartDCs-NCL+anti–PD-L1 peptide (**Fig. 4D**, lane 4) > SmartDCs-NCL (**Fig. 4D**, lane 3). The increased autophagy reduced BAX and restored expression of BAX in SmartDCs-NCL+RPS3+curcumin (**Fig. 4D**, lane 9) was detected more than those in SmartDCs-NCL+RPS3+anti–PD-L1 peptide (**Fig. 4D**, lane 8) and SmartDCs-NCL+RPS3 (**Fig. 4D**, lane 7) in both MDA-MB-231 and MCF-7. The quantitated results of these molecules were summarized (**Fig. 4F** and **I**). The curcumin stimulated NCL-specific T-cell killing against TNBC cells not only by BAX/BCL-2 induction, but also by PD-L1 degradation through the autophagy formation indicated by the decreased p62 and PD-L1 levels (**Fig. 4G** and **H**, lanes 5 and 9).

To test whether autophagy could involve NCL-specific T-cell toxicity, the treatment of spautin-1 that can induce the destabilization of BECLIN-1–dependent autophagy (30) was performed. Reduction of LC3 and BAX was detected that demonstrated the prevention of cell death by NCL-specific T cells along with increased PD-L1 (**Fig. 4D** and **H**, lanes 6 and 10) compared with that of NCL-specific T cells combined with anti–PD-L1 peptide (lanes 4 and 8) or curcumin (**Fig. 4D** and **H**, lanes 5 and 9). In MCF-7 cells, the levels of LC3-II (**Fig. 4F**, lanes 5 and 9) and BAX (**Fig. 4I**, lanes 5 and 9) were increased only in the cells cultivated in the combination of curcumin with NCL-specific T cells activated by SmartDCs-NCL (**Fig. 4F**, lane 5) and SmartDCs-NCL+RPS3 (**Fig. 4F**, lane 9). Of note, no significant differences of p62 expression between treatments were found (**Fig. 4G**, lanes 5 and 9).

Spautin-1 prevents the induction of autophagy and apoptosis by NCL-specific T cells

The clonogenic assay confirmed the effect of autophagy modulators–mediated NCL-specific T-cell–induced cell death. Importantly, that spautin-1 could rescue a colony formation of cancer cells co-cultured with NCL-specific T cells demonstrated the reduction of cell availability in a dose-dependent manner to the E:T ratio (**Fig. 5A** and **B**; Supplementary Fig. S4A). The double staining demonstrated that apoptosis (BAX-positive) was ensured in the same cells in which autophagy (LC3-positive) was induced in NCL-specific T cells activated by SmartDCs-NCL or SmartDCs-NCL+RPS3 combined with either anti–PD-L1 peptide or curcumin (**Fig. 5C**). Spautin-1 limited the expression of the pro-apoptotic BAX protein induced by NCL-specific T cells and largely prevented autophagosome formation (**Fig. 5C**; Supplementary Fig. S4B–S4C). Moreover, on the basis of

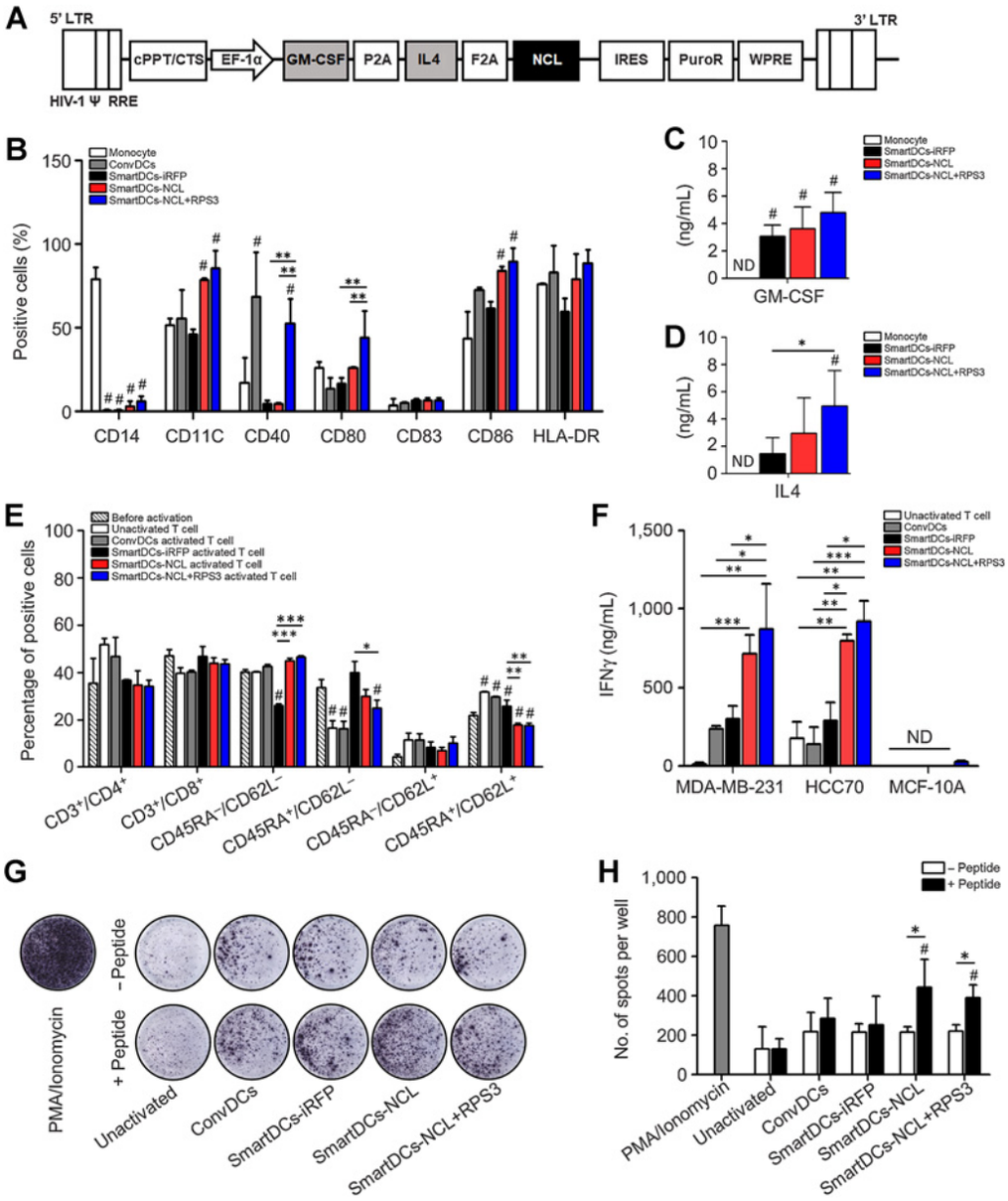

Figure 2.

Production of SmartDCs-NCL and NCL-specific T cells. **A,** Schematic representation of the tricistronic lentiviral construct SmartDCs-NCL containing GM-*CSF*, *IL-4,* and *NCL* genes. The chimeric 5′ long terminal repeat (LTR), the packaging signal (ψ), the truncated and the Rav responsive element (RRE), the central polypurine and termination sequence (cPPT) are indicated. The SmartDCs–NCL construct contains 2A-like self-cleaving sequences and PuroR indicates puromycin resistance gene. **B,** Percentage of positive cells represented immunophenotypes of monocytes and DC markers. **C** and **D,** Average GM-CSF and IL-4 cytokines released in supernatants of monocytes (day 0), DCs transduced with tricistronic Lentivirus (day 7), determined by ELISA summarized from two independent experiments. **E,** T-cell subsets before activation (day 0) and after day 15 that were activated by unactivated T cells (white bar), ConvDCs activated T cells (gray bar), SmartDCs–iRFP-activated T cells (black bar), SmartDCs–NCL-activated T cells (red bar), and SmartDCs-NCL+RPS3–activated T cells (blue bar). T cells were classified as terminal effector T cells (T_{EM}; $CD3^+$, $CD8^+$, $CD45RA^-$, and $CD62L^-$), effector memory T cells (T_{EMRA}; $CD3^+$, $CD8^+$, $CD45RA^+$, and $CD62L^-$), central memory T cells (T_{CM}; $CD3^+$, $CD8^+$, $CD45RA^-$, and $CD62L^+$) and naive T cells (T_N; $CD3^+$, $CD8^+$, $CD45RA^+$, and $CD62L^+$). **F,** IFNγ secretion of unactivated T cells, ConvDCs, SmartDCs-iRFP, SmartDCs-NCL, and SmartDCs-NCL+RPS3-activatedmT cells upon co-culture with indicated target cell lines at E:T ratio of 10:1 for 24 hours quantitated by IFNγ ELISA. **G** and **H,** IFNγ production of specific T cells in response to corresponding NCL peptide was measured by ELISpot assay. The image and number of spots was counted using the BIOREADER5000 Pro F and the CellCounter software (Nghia, Ho) version 0.2.1, with each experiment performed in triplicated with 1×10^5 cells of activated T lymphocytes per well and the average number of the spots was calculated. PMA; Phorbol 12-myristate 13-acetate. Original magnifications of ×200. Data are shown as mean±SD. *, $P < 0.05$; **, $P < 0.01$ and ***, $P < 0.001$ compared with monocytes; #, $P < 0.05$; compared with monocytes or before activation conditioned or compared with unpulsed peptide. All data shown were reproduced in three separate experiments.

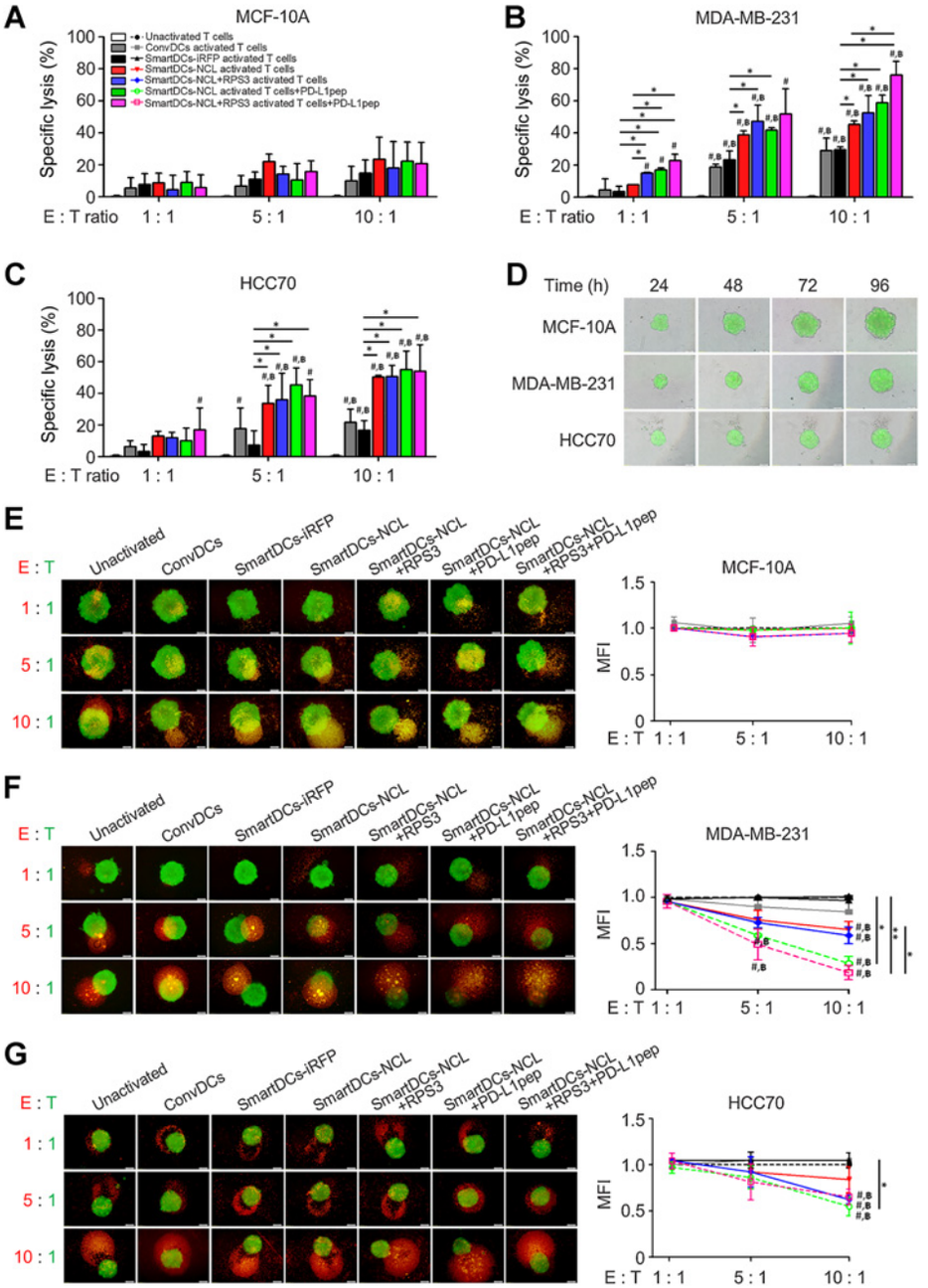

Figure 3.

Cytotoxic assay of NCL-specific T cells plus anti–PD-L1 peptide (anti–PD-L1pep) against TNBC cells. The indicated MDA-MB-231, HCC70, and MCF-10A were co-cultured with T cells activated with SmartDCs systems, including SmartDCs-iRFP, SmartDCs-NCL, SmartDCs-NCL+RPS3, SmartDCs-NCL plus anti–PD-L1 peptide or SmartDCs-NCL+RPS3 plus anti–PD-L1 peptide. **A–C,** Percentage of specific lysis of MDA-MB-231 **(A)**, HCC70 **(B),** and MCF-10A **(C)** measured as mWasabi and CMRA fluorescence-labeled viable cells by Pierce Firefly Luciferase Glow Assay Kit at effector T cells to target cells (E:T) ratios, 1:1, 5:1, and 10:1. **D,** 3-D spheroids monitored at 24, 48, 72, and 96 hours. **E–G,** Fluorescence images of mWasabi and CMRA fluorescence-labeled viable 3D-spheroids co-cultured with T cells activated by SmartDCs-iRFP, SmartDCs-NCL, SmartDCs-NCL+RPS3, SmartDCs-NCL plus anti–PD-L1 peptide or SmartDCs-NCL+RPS3 plus anti–PD-L1 peptide compared with unactivated T cells and ConvDCs. Mean fluorescence intensity (MFI) relative to spheroid treated with unactivated T cells at 24 hours after treatment were calculated and plotted at E:T of 1:1, 5:1, and 10:1. Scale bar, 100 μm; original magnifications of ×100. *, $P < 0.05$; **, $P < 0.01$; and ***, $P < 0.001$. #, $P < 0.05$ compared with unactivated T cells conditioned; ฿, $P < 0.05$ compared with E:T ratio 1:1 of each treatment. All images shown are representative of at least three separate experiments.

the CellTracker viability in 3-D spheroids, spautin-1 treatment reversed the killing effect of NCL-specific T cells (**Fig. 5D**; Supplementary Fig. S4D and S4E).

Discussion

Many preclinical studies have demonstrated the use of antigen-specific T cells stimulated by DCs as promising immunotherapeutic approaches for the treatment of patients with cancers such as metastatic renal cell carcinoma (31), melanoma (32), cholangiocarcinoma (7), and breast cancer (7). ConvDCs generated from PBMC, however, require a standard method with clinical-grade laboratory cytokines that are costly (4–6). The limited effectiveness of poor consistency and low viability of ConvDCs leading to the insufficient numbers of $CD8^+$ cytotoxic T lymphocytes was reported (33). To overcome these limitations, SmartDCs carrying cytokines needed for self-differentiation and antigen-encoding genes for antigen production and intracellular presentation onto the HLA molecules on DCs were introduced (5–7, 32, 34). NCL confirmed its impact as a tumor-associated antigen with its high expression in TNBC samples and revealed a significant correlation with short patient survival time. SmartDCs-NCL was performed and in combination with recombinant RPS3 could significantly induce NCL-specific T-cell activation to kill NCL^{High} TNBC cells. From the evidence, the anti–PD-L1 peptide or an

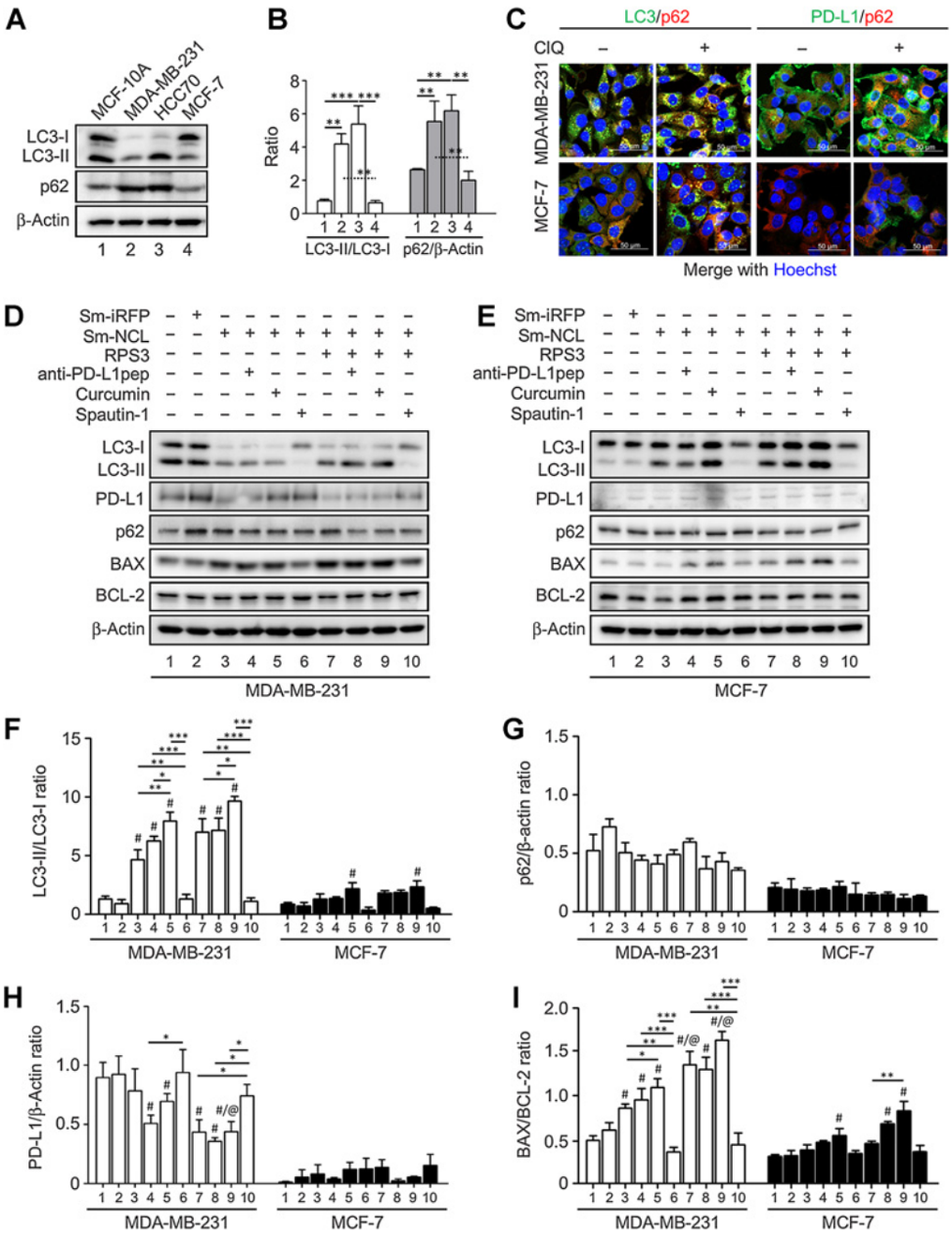

Figure 4.

Expression of apoptosis- and autophagy-related proteins in MDA-MB-231 cells exposed to NCL-specific T cells plus anti–PD-L1 peptide (anti–PD-L1pep) or curcumin. **A,** The expressions of LC3-I, LC3-II and p62 were detected by Western blotting analysis (one of the three is shown). **B,** Densitometry data of three independent experiments are shown in the histogram as mean ± SD. **C,** Double immunofluorescence staining for LC3 (green fluorescence) or PD-L1 (green fluorescence) and p62 (red fluorescence) in MDA-MB-231 and MCF-7 cells adherent on coverslips cultured 24 hours. Chloroquine (ClQ) was added to discriminate between true induction of autophagy and blocking of the autophagy flux. Nuclei were counterstained with Hoechst33342 (blue fluorescence). Scale bar, 20 μm; magnifications, ×630. Representative images of three independent experiments. **D** and **E,** MDA-MB-231 and **(D)** MCF-7 cells **(E)** were co-cultured with T cells activated with SmartDC systems in the presence of anti–PD-L1 peptide (50 μmol/L) or curcumin (30 μmol/L) or spautin-1 (10 μmol/L), were detected by Western blot analysis for LC3-I, LC3-II, PD-L1, p62, BA, and BCL-2 proteins. β-Actin is used as a marker of protein loading. **F–I,** Densitometry of Western blotting data are reported as mean ± SD. *, $P < 0.05$; **, $P < 0.01$; and ***, $P < 0.001$; $^{\#}$, $P < 0.05$ compared with untreated cells (lane 1); $^{@}$, $P < 0.05$ comparisons between with or without RPS3 addition.

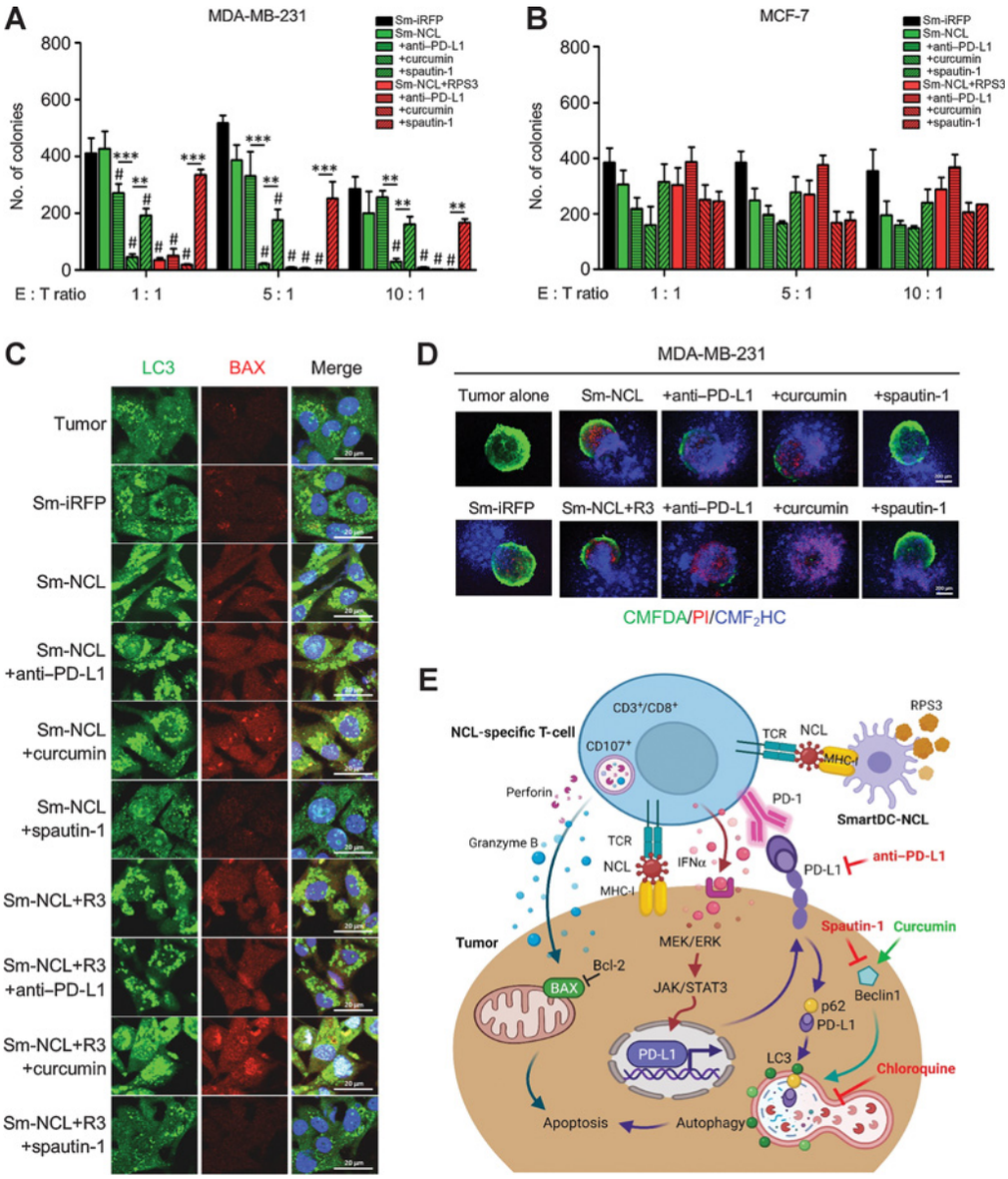

Figure 5.

Curcumin-mediated destabilization of PD-L1 through the induction of autophagy and NCL-specific T-cell activity enhancement. **A** and **B,** The number of colony formation assays of MDA-MB-231 and MCF-7 incubated in NCL-specific T cells with or without anti–PD-L1 peptide (anti–PD-L1pep) or curcumin or spautin-1. **C,** Cells adherent on coverslips were incubated as described previously, cells were fixed and stained with LC3 (green fluorescence, as marker of autophagic vacuoles) and BAX (red fluorescence, as marker of apoptosis). Nuclei were counterstained with Hoechst33342 (blue fluorescence). Scale bar, 20 μm; magnifications, ×630. **D,** CellTracker CMFDA–labeled 3-D spheroid (MDA-MB-231) cells in a low attachment plate were stained with propidium iodine (PI) demonstrated cell death activation after co-cultured with CellTracker CMF_2HC labeled NCL-specific T cells in present of anti–PD-L1 peptide or curcumin or spautin-1. The represented images were captured at E:T ratio, 10:1 for 24 hours. Scale bar, 20 μm; magnifications, ×630. **E,** Proposed mechanism of autophagy and apoptosis-mediated SmartDCs-NCL–activated T cells: (i) the addition of RPS3 enhanced the maturation and activation of SmartDCs-NCL; (ii) leads to the successful NCL-specific T-cell generation; (iii) with effectively recognized and killed NCL^{High}/$PD\text{-}L1^{High}$ TNBC cells. **, $P < 0.01$ and ***, $P < 0.001$; #, $P < 0.05$ compared with SmartDCs-NCL. All imaging studies were replicated in at least three independent experiments.

autophagy modulator curcumin could notably sensitize NCL-specific T cells against NCL^{High}/$PD\text{-}L1^{High}$ TNBC cells.

There is now growing evidence of the clinical perspective that self-differentiated DCs showed greater viability and immune potency *in vitro* and *in vivo* than traditionally generated DCs, in the absence of exogenous cytokines (35, 36). Importantly, T-cell stimulation was more consistent in immunogenic capability of MHC class I–restricted antigen presentation for SmartDCs (37). This evidence supports the currently used SmartDCs-NCL having features of reduction of CD14 and increments of CD11c, CD40, CD80, CD83, CD86, and HLA-DR. On the basis of the recent study that RPS3 was bound to TLR4 and activated DCs (38). To generate the maturated and activated DCs, LPS,

a well-known TLR4 ligand, has a significant effect on inducing maturation and activation of DCs; however, LPS is not appropriate for use in humans because it is an endotoxin. Instead, the TLR9 ligand CpG, or the TLR3 ligand I:C, are commonly used, but large amounts are required to induce DC maturation and activation (8, 38). Therefore, to explore a new TLR4 ligand, RPS3 is needed, which is screened from human tumor cells. Moreover, DC vaccination with the newly discovered TLR4 ligand, RPS3, has recently been confirmed as an adjuvant to activate DC maturation (8). RPS3 as an exogenous adjuvant for further SmartDCs maturation showed up-expression of CD40 and CD80, and secretion of GM-CSF and IL-4. The numbers of the effector memory T cells (T_{EM}, $CD3^+/CD8^+/CD45RA^-/CD62L^-$) and tumor-specific $CD8^+IFN\gamma^+$ T cells were increased by SmartDCs-NCL or SmartDCs-NCL plus RPS3 activation. The specific effect of NCL-overexpressing tumor cell killing could be achieved using either SmartDCs-NCL or SmartDCs-NCL with RPS3 as an adjuvant.

As a 3-D cell culture, mimic solid tumors in the case of oncological studies (39), spheroids represent a promising technique to improve the function, differentiation and viability as compared with conventional 2-D cultures (40). Here, *in vitro* multicellular spheres adapted in tumor growth for T cells killing assays are focused on. The cell suspension was cultivated in low-adherent conditions and complete media with 10% FBS to promote extensive proliferation and was devoid of cancer stem cell enrichment (41).

Clinical trials for cancer immunotherapy, including immune checkpoint inhibitor therapy, have been conducted worldwide (42, 43). Therefore, it is expected that the better effect of using PD-L1 modulator together with NCL-specific T cells. Anti–PD-L1 peptide (CLQKTPKQC) has been screened by phage-displayed peptide libraries with a high affinity and efficiency blocks the interaction between PD-L1 and PD-1 in MDA-MB-231 and MCF-7 cells (24). Recently, autophagy has been reported to influence PD-L1 levels (17, 44). The significant overexpression of NCL in patients with TBNC and established the production of NCL-specific T cells aimed to use as a new treatment in patients with TNBC was demonstrated. Most of the NCL-positive cancer cells, however, expressed high PD-L1 that can reduce cancer cell destruction function of T cells. Hence, it is considered of great interest to show that an anti–PD-L1 peptide can help attenuate this effect. Results of this current study confirm the benefit of the combined anti–PD-L1 peptide and NCL-specific T cells over either NCL-specific T cells or anti–PD-L1 peptide alone (Supplementary Fig. S4A). The alteration of the autophagy pathway can stimulate or limit the potent immune responses that have been reported; however, the mechanism has remained unclear (45). Failure of autophagy contributed to a limitation of the T-lymphocyte attack on TNBC (19). Resveratrol, autophagy inducer, pre-treated MDA-MB-231 cells were more sensitive to T-cell–mediated cytotoxicity (19). Treatment with an autophagy inducer, the natural compound "curcumin," or in combination with anti–PD-L1 antibody attenuated PD-L1 expression and enhanced T-cell responses against bladder cancer (21) and tongue squamous cell carcinoma (46). This evidence supports current findings that SmartDCs-NCL and SmartDCs-NCL plus RPS3-activated NCL-specific T cells could sensitize $NCL^{High}/PD\text{-}L1^{High}$ MDA-MB-231 cell killing when used in combination with anti–PD-L1 peptide or curcumin.

Treatment with curcumin before SmartDCs-NCL and SmartDCs-NCL plus RPS3 application showed high LC3 and low p62 expression that could be interpreted as an efficient autophagy flux. Chloroquine or ClQ, is a well-established chemical able to interrupt the degradation of autophagosomes, as testified by several scientific reports (27). The degradation of PD-L1 via autophagy pathway has been reported (47, 48). It was herein noticed that the addition of ClQ could inhibit autophagosome degradation; thus, concerning the phenomena here described, the increased expression of PD-L1 ensures that PD-L1 was practically processed in autophagosome accumulation. Hence, PD-L1 can be degraded via the selective autophagy–lysosome pathway that facilitated recognition by p62/QSQTM1, autophagy substrate (47, 48). The ClQ treatment was performed to confirm the effect of PD-L1 degraded by autophagy. The inhibition of autophagy by ClQ was not expected to increase the activity of stimulated T cells; therefore, the condition of additive of ClQ was not required. Moreover, the hyper-induction of autophagy by SmartDCs-NCL, SmartDCs-NCL plus RPS3, SmartDCs-NCL/RPS3/anti–PD-L1 peptide, and SmartDCs-NCL/RPS3/curcumin led to apoptosis of breast cancer cells. In fact, this effect was abolished when autophagy was inhibited by spautin-1, through promoting the ubiquitin-mediated degradation of BECLIN-1 (30). Spautin-1 abrogated the induction of autophagy by SmartDCs-NCL as shown by the lack of formation of LC3-II. As predictable, spautin-1 inhibited autophagy and rescues PD-L1 expression. The current study results provide evidence supporting the potential mechanisms of autophagy-dependent apoptosis of TNBC cells that were obtained with treatment of NCL-specific T cells activated by SmartDCs-NCL. Enhancement of SmartDCs-NCL activity by RPS3 could be greatly increased NCL-specific T cells with high IFNγ production. The degradation of PD-L1–linked ubiquitination of p62 might be critical for a selective autophagy pathway to enhance NCL-specific T cells against $NCL^{High}/PD\text{-}L1^{High}$ cells. Mechanistically, the reduction of p62 in cancer cells could attenuate PD-L1 induction by autophagy inhibition, implying that autophagy regulates PD-L1 expression through the p62 pathway (47). Notably, induction of autophagy sensitized TNBC cells to NCL-specific T-cell–mediated tumor killing similar to the improvement of anticancer effects of NCL-specific T cells by immune checkpoint inhibitor (**Fig. 5E**).

In conclusion, autophagy contributes to the anticancer ability of NCL-specific T cells activated by SmartDCs-NCL mechanistically through both apoptotic and autophagic cell death pathways. It is possible to provide clinical approaches by targeting $NCL^{High}/PD\text{-}L1^{High}$ TNBC by NCL-specific T cells in combination with a PD-L1 inhibitor or autophagic stimulator. These approaches may highlight the potential of using NCL-specific T cells in patients with cancer featured with a high NCL level, and anti–PD-L1 molecules (anti–PD-L1 peptide or PD-L1 suppression through an autophagy stimulator) to sensitize T cells killing functions against NCL and PD-L1–expressing cancer cells.

Authors' Disclosures

No disclosures were reported.

Authors' Contributions

S. Thongchot: Conceptualization, data curation, software, formal analysis, investigation, writing–original draft, writing–review and editing. **N. Jirapongwattana:** Data curation, investigation, methodology. **P. Luangwattananun:** Data curation, methodology. **W. Chiraphapphaiboon:** Data curation, methodology. **N. Chuangchot:** Data curation, methodology. **D. Sa-nguanraksa:** Resources. **P. O-Charoenrat:** Resources. **P. Thuwajit:** Conceptualization, methodology. **P. Yenchitsomanus:** Conceptualization, resources, methodology. **C. Thuwajit:** Conceptualization, resources, supervision, funding acquisition, methodology, writing–original draft, project administration, writing–review and editing.

Acknowledgments

This research project was supported by Mid-Career Research Grant, The National Research Council of Thailand (grant no. RSA6280091), Ministry of Higher Education, Science, Research and Innovation, Thailand (to C. Thuwajit) and New Researcher Grant, Mahidol University (to S. Thongchot). The financial support from Siriraj

Research Grant, Faculty of Medicine Siriraj Hospital, Mahidol University and The National Research Council of Thailand 2020. Thanks are due to Prof. Somchai Pinlaor (Khon Kaen University, Thailand) for kind offer of curcumin; Prof. Ciro Isidoro (Università del Piemonte Orientale "A. Avogadro," Italy) for kind provision of spautin-1. Special thanks to Surat Phumphuang for clinical data collection. The authors would like to thank Prof. James A. Will, USA for the English edition.

The costs of publication of this article were defrayed in part by the payment of page charges. This article must therefore be hereby marked *advertisement* in accordance with 18 U.S.C. Section 1734 solely to indicate this fact.

Received October 7, 2021; revised December 21, 2021; accepted March 2, 2022; published first March 21, 2022.

References

1. Dass SA, Tan KL, Selva Rajan R, Mokhtar NF, Mohd Adzmi ER, Wan Abdul Rahman WF, et al. Triple-negative breast cancer: a review of present and future diagnostic modalities. Medicina 2021;57:62.
2. Bianchini G, Balko JM, Mayer IA, Sanders ME, Gianni L. Triple-negative breast cancer: challenges and opportunities of a heterogeneous disease. Nat Rev Clin Oncol 2016;13:674–90.
3. Marra A, Viale G, Curigliano G. Recent advances in triple-negative breast cancer: the immunotherapy era. BMC Med 2019;17:90.
4. Engell-Noerregaard L, Hansen TH, Andersen MH, thor Straten P, Svane IM. Review of clinical studies on dendritic cell-based vaccination of patients with malignant melanoma: assessment of correlation between clinical response and vaccine parameters. Cancer Immunol Immunother 2009;58:1.
5. Sundarasetty B, Chan L, Darling D, Giunti G, Farzaneh F, Schenck F, et al. Lentivirus-induced 'Smart'dendritic cells: pharmacodynamics and GMP-compliant production for immunotherapy against TRP2-positive melanoma. Gene Ther 2015;22:707–20.
6. Pincha M, Sai Sundarasetty B, Salguero G, Gutzmer R, Garritsen H, Macke L, et al. Identity, potency, *in vivo* viability, and scaling up production of lentiviral vector–induced dendritic cells for melanoma immunotherapy. Hum Gene Ther Methods 2012;23:38–55.
7. Panya A, Thepmalee C, Sawasdee N, Sujjitjoon J, Phanthaphol N, Junking M, et al. Cytotoxic activity of effector T cells against cholangiocarcinoma is enhanced by self-differentiated monocyte-derived dendritic cells. Cancer Immunol Immunother 2018;67:1579–88.
8. Park HJ, Jang GY, Kim YS, Park JH, Lee SE, Vo MC, et al. A novel TLR4 binding protein, 40S ribosomal protein S3, has potential utility as an adjuvant in a dendritic cell-based vaccine. J Immunother Cancer 2019;7:1–13.
9. Xu JY, Lu S, Xu XY, Hu SL, Li B, Li WX, et al. Prognostic significance of nuclear or cytoplasmic nucleolin expression in human non–small cell lung cancer and its relationship with DNA-PKcs. Tumor Biol 2016;37:10349–56.
10. Qi J, Li H, Liu N, Xing Y, Zhou G, Wu Y, et al. The implications and mechanisms of the extra-nuclear nucleolin in the esophageal squamous cell carcinomas. Med Oncol 2015;32:45.
11. Rosenberg JE, Bambury RM, Van Allen EM, Drabkin HA, Lara PN, Harzstark AL, et al. A phase II trial of AS1411 (a novel nucleolin-targeted DNA aptamer) in metastatic renal cell carcinoma. Invest New Drugs 2014;32:178–87.
12. Mongelard F, Bouvet P. AS-1411, a guanosine-rich oligonucleotide aptamer targeting nucleolin for the potential treatment of cancer, including acute myeloid leukemia. Curr Opin Mol Ther 2010;12:107–14.
13. Soundararajan S, Chen W, Spicer EK, Courtenay-Luck N, Fernandes DJ. The nucleolin targeting aptamer AS1411 destabilizes Bcl-2 messenger RNA in human breast cancer cells. Cancer Res 2008;68:2358–65.
14. Laber D, Taft B, Kloecker G, Acton G, Miller D. Pharmacokinetics of the anti-nucleolin aptamer AS1411 in a phase I study. AACR; 2007.
15. Pichiorri F, Palmieri D, De Luca L, Consiglio J, You J, Rocci A, et al. *In vivo* NCL targeting affects breast cancer aggressiveness through miRNA regulation. J Exp Med 2013;210:951–68.
16. Fonseca NA, Rodrigues AS, Rodrigues-Santos P, Alves V, Gregório AC, Valério-Fernandes Â, et al. Nucleolin overexpression in breast cancer cell sub-populations with different stem-like phenotype enables targeted intracellular delivery of synergistic drug combination. Biomaterials 2015;69:76–88.
17. White E, DiPaola RS. The double-edged sword of autophagy modulation in cancer. Clin Cancer Res 2009;15:5308–16.
18. Tang H, Sebti S, Titone R, Zhou Y, Isidoro C, Ross TS, et al. Decreased BECN1 mRNA expression in human breast cancer is associated with estrogen receptor-negative subtypes and poor prognosis. EBioMedicine 2015;2:255–63.
19. Li ZL, Zhang HL, Huang Y, Huang JH, Sun P, Zhou NN, et al. Autophagy deficiency promotes triple-negative breast cancer resistance to T-cell–mediated cytotoxicity by blocking tenascin-C degradation. Nat Commun 2020;11:1–19.
20. Maher CM, Thomas JD, Haas DA, Longen CG, Oyer HM, Tong JY, et al. Small-molecule sigma1 modulator induces autophagic degradation of PD-L1. Mol Cancer Res 2018;16:243–55.
21. Shao Y, Zhu W, Da J, Xu M, Wang Y, Zhou J, et al. Bisdemethoxycurcumin in combination with α–PD-L1 antibody boosts immune response against bladder cancer. Onco Targets Ther 2017;10:2675.
22. Chen X, Lu Y, Zhang Z, Wang J, Yang H, Liu G. Intercellular interplay between Sirt1 signalling and cell metabolism in immune cell biology. Immunology 2015;145:455–67.
23. Yang Y-CS, Li Z-L, Shih Y-J, Bennett JA, Whang-Peng J, Lin H-Y, et al. Herbal medicines attenuate PD-L1 expression to induce anti-proliferation in obesity-related cancers. Nutrients 2019;11:2979.
24. Gurung S, Khan F, Gunassekaran GR, Yoo JD, Poongkavithai Vadevoo SM, Permpoon U, et al. Phage display-identified PD-L1-binding peptides reinvigorate T-cell activity and inhibit tumor progression. Biomaterials 2020;247:119984.
25. Cailleau R, Young R, Olive M, Reeves WJ Jr. Breast tumor cell lines from pleural effusions. J Natl Cancer Inst 1974;53:661–74.
26. Gazdar AF, Kurvari V, Virmani A, Gollahon L, Sakaguchi M, Westerfield M, et al. Characterization of paired tumor and non-tumor cell lines established from patients with breast cancer. Int J Cancer 1998;78:766–74.
27. Klionsky DJ, Abdel-Aziz AK, Abdelfatah S, Abdellatif M, Abdoli A, Abel S, et al. Guidelines for the use and interpretation of assays for monitoring autophagy. Autophagy 2021;17:1–382.
28. Sumransub N, Jirapongwattana N, Jamjuntra P, Thongchot S, Chieochansin T, Yenchitsomanus PT, et al. Breast cancer stem cell RNA□pulsed dendritic cells enhance tumor cell killing by effector T cells. Oncol Lett 2020;19:2422–30.
29. Mangare C, Tischer-Zimmermann S, Riese SB, Dragon AC, Prinz I, Blaszczyk R, et al. Robust identification of suitable T-cell subsets for personalized CMV-specific T-cell immunotherapy using CD45RA and CD62L microbeads. Int J Mol Sci 2019;20:1415.
30. Liu J, Xia H, Kim M, Xu L, Li Y, Zhang L, et al. Beclin1 controls the levels of p53 by regulating the deubiquitination activity of USP10 and USP13. Cell 2011;147:223–34.
31. Flörcken A, Kopp J, Van Lessen A, Movassaghi K, Takvorian A, Jöhrens K, et al. Allogeneic partially HLA-matched dendritic cells pulsed with autologous tumor cell lysate as a vaccine in metastatic renal cell cancer: a clinical phase I/II study. Hum Vaccin Immunother 2013;9:1217–27.
32. Koya RC, Kimura T, Ribas A, Rozengurt N, Lawson GW, Faure-Kumar E, et al. Lentiviral vector–mediated autonomous differentiation of mouse bone marrow cells into immunologically potent dendritic cell vaccines. Mol Ther 2007;15:971–80.
33. Lou Y, Wang G, Lizée G, Kim GJ, Finkelstein SE, Feng C, et al. Dendritic cells strongly boost the antitumor activity of adoptively transferred T cells *in vivo*. Cancer Res 2004;64:6783–90.
34. Breckpot K, Heirman C, Neyns B, Thielemans K. Exploiting dendritic cells for cancer immunotherapy: genetic modification of dendritic cells. The Journal of Gene Medicine: a cross-disciplinary journal for research on the science of gene transfer and its clinical applications. J Gene Med 2004;6:1175–88.
35. Basak SK, Harui A, Stolina M, Sharma S, Mitani K, Dubinett SM, et al. Increased dendritic cell number and function following continuous *in vivo* infusion of granulocyte macrophage–colony-stimulating factor and interleukin-4. Blood 2002;99:2869–79.
36. Roth MD, Gitlitz BJ, Kiertscher SM, Park AN, Mendenhall M, Moldawer N, et al. Granulocyte macrophage colony-stimulating factor and interleukin 4 enhance the number and antigen-presenting activity of circulating $CD14^+$ and $CD83^+$ cells in cancer patients. Cancer Res 2000;60:1934–41.

37. Koya RC, Weber JS, Kasahara N, Lau R, Villacres MC, Levine AM, et al. Making dendritic cells from the inside out: lentiviral vector-mediated gene delivery of granulocyte-macrophage colony-stimulating factor and interleukin 4 into $CD14^{+}$ monocytes generate dendritic cells in vitro. Hum Gene Ther 2004;15: 733–48.
38. Lu YC, Yeh WC, Ohashi PS. LPS/TLR4 signal transduction pathway. Cytokine 2008;42:145–51.
39. Li CL, Tian T, Nan KJ, Zhao N, Guo YH, Cui J, et al. Survival advantages of multicellular spheroids vs. monolayers of HepG2 cells in vitro. Oncol Rep 2008; 20:1465–71.
40. Godoy P, Hengstler JG, Ilkavets I, Meyer C, Bachmann A, Müller A, et al. Extracellular matrix modulates sensitivity of hepatocytes to fibroblastoid dedifferentiation and transforming growth factor β–induced apoptosis. Hepatology 2009;49:2031–43.
41. Weiswald LB, Bellet D, Dangles-Marie V. Spherical cancer models in tumor biology. Neoplasia 2015;17:1–15.
42. Schmid P, Adams S, Rugo HS, Schneeweiss A, Barrios CH, Iwata H, et al. Atezolizumab and nab-paclitaxel in advanced triple-negative breast cancer. N Engl J Med 2018;379:2108–21.
43. Asahara S, Takeda K, Yamao K, Maguchi H, Yamaue H. Phase I/II clinical trial using HLA-A24–restricted peptide vaccine derived from KIF20A for patients with advanced pancreatic cancer. J Transl Med 2013;11:1–13.
44. Klionsky DJ. Autophagy. Curr Biol 2005;15:R282–R3.
45. Amaravadi RK. Autophagy in tumor immunity. Science 2011;334:1501–2.
46. Liao F, Liu L, Luo E, Hu J. Curcumin enhances antitumor immune response in tongue squamous cell carcinoma. Arch Oral Biol 2018;92:32–7.
47. Wang X, Wu WK, Gao J, Li Z, Dong B, Lin X, et al. Autophagy inhibition enhances PD-L1 expression in gastric cancer. J Exp Clin Cancer Res 2019;38: 1–14.
48. Zhang J, Dang F, Ren J, Wei W. Biochemical aspects of PD-L1 regulation in cancer immunotherapy. Trends Biochem Sci 2018;43:1014–32.